Journal of Alloys and Compounds 509 (2011) 3913–3916

Contents lists available at ScienceDirect

Journal of Alloys and Compounds

journal homepage: www.elsevier.com/locate/jallcom

Microstructure and martensitic transformation of cast TiNiSi shape memory alloys

Kh.M. Ibrahim [a], N. Elbagoury [a,b,*], Y. Fouad [c]

[a] CMRDI, P.O. Box 87, Helwan, Cairo, Egypt
[b] Chemistry Department, Faculty of Science, TAIF University, P.O. Box 888, El-Haweyah, El-Taif, Saudi Arabia
[c] GUC, Cairo, Egypt

ARTICLE INFO

Article history:
Received 25 November 2010
Received in revised form
18 December 2010
Accepted 22 December 2010
Available online 29 December 2010

Keywords:
TiNiSi shape memory alloys
Microstructure
Second phase
Martensitic phase transformation
Hardness measurements

ABSTRACT

The martensitic transformation behavior, second phases and hardness of $Ti_{51}Ni_{49-x}Si_x$ shape memory alloys (SMAs) with $x = 0$, 1 and 2 at.% are investigated. The transformation temperature of one stage martensitic reaction B2 ↔ B19′ is associated with the forward (M_s) and reverse (A_s) martensitic transformations, respectively. All experimental DSC results such as martensitic transformation peaks (M^*) and reverse martensitic transformation peaks (A^*) are increased and became sharper with increasing Si-content. The microstructure investigation of the studied SMAs ($Ti_{51}Ni_{49-x}Si_x$) showed that there are two types of precipitated second phase particles. The first one is Ti_2Ni which mainly located at grain boundaries and intermetallic compound of $Ti_2(Ni + Si)$ phase distributed inside the matrix. The volume fraction of these two phases is increased with Si content. Additionally, a small amount of Si remained in solid solution of the matrix of $Ti_{51}Ni_{49-x}Si_x$ SMAs. Moreover, hardness of $Ti_{51}Ni_{49-x}Si_x$ SMAs is increased as the Si-content increases.

1. Introduction

In recent years, there has been growing interest in the use of TiNi shape memory alloys (SMAs) as functional/smart materials for a variety of applications [1–3]. This material (TiNi) is also often called and marked as Ti–Ni, Ni–Ti or Nitinol. Ni–Ti can restructure itself from a B2 austenite phase (A), to a B19′ martensite phase through a decrease in temperature or increase in applied stress [3]. However under certain circumstances, which depends on thermal and mechanical effects such as thermal cycling, heat treatment, chemical composition, deformation, etc., an inter mediate phase, known as rhombohedral or R-phase (denoted by R), may appear between austenite transforming to martensite, resulting in a two-stage transformation [3–5].

Development of SMAs for commercial applications has led to add ternary elements such as palladium, platinum, hafnium or zirconium to NiTi for which the transformation temperatures can be shifted anywhere in the range of 100–800 °C [6]. An addition of a third element to replace Ni and/or Ti has a substantial effect on phase transformation behavior of TiNi alloys [7,8]. The starting temperature of martensitic transformation, M_s, of TiNi binary alloys decreases following the substitution of Ni with V, Cr, Mn, Fe or Co elements [9–11]. However, the M_s increases remarkably following the substitution of Ni with Au, Pd or Pt in amounts not less than 15–20 at.% [12–14].

For binary TiNi shape memory alloys, most research work has been devoted to the equiatomic or Ni-rich TiNi alloys, while few systematical studies are reported on Ti-rich TiNi alloys. The present awareness of Ti-rich TiNi alloys is that they contain precipitated phase of Ti_2Ni and have higher transformation temperatures compared with the equiatomic or Ni-rich TiNi alloys [15,16]. However, the phase transformation behavior and shape memory effect (SME) of Ti-rich TiNi alloys have not been clarified thoroughly.

In this work, the transformation behavior upon heating and cooling was studied by a calorimetric to reveal the relationship between chemical composition and transformation characteristics of three different TiNi SMAs. Three $Ti_{51}Ni_{49-x}Si_x$ alloys with different Si contents were studied by differential scanning calorimetry (DSC) method and X-ray diffraction (XRD). On the basis of the results, the effect of Si on the martensitic transformation of the $Ti_{51}Ni_{49-x}Si_x$ alloys was discussed.

2. Experimental work

Conventional tungsten arc melting under vacuum technique was used to prepare three different TiNi shape memory alloys. The composition of these alloys are Ti_{51}–Ni_{49}, Ti_{51}–Ni_{48}–Si_1 and Ti_{51}–Ni_{47}–Si_2 (at.%). These alloys were cast as a disc form with 40 mm diameter and 10 mm thickness. Each disc was cut into four equal pieces for metallurgical investigations. A quantitative chemical analysis of these alloys was performed by using electron probe micro-analyzer equipped with a wavelength dispersive X-ray spectrometer analysis system. The microstructure of the investi-

* Corresponding author at: Chemistry Department, Faculty of Science, TAIF University, P.O. Box 888, El-Haweyah, El-Taif, Saudi Arabia. Tel.: +966 596264584.
E-mail address: nader_elbagoury@yahoo.com (N. Elbagoury).

0925-8388/$ – see front matter © 2010 Elsevier B.V. All rights reserved.
doi:10.1016/j.jallcom.2010.12.164

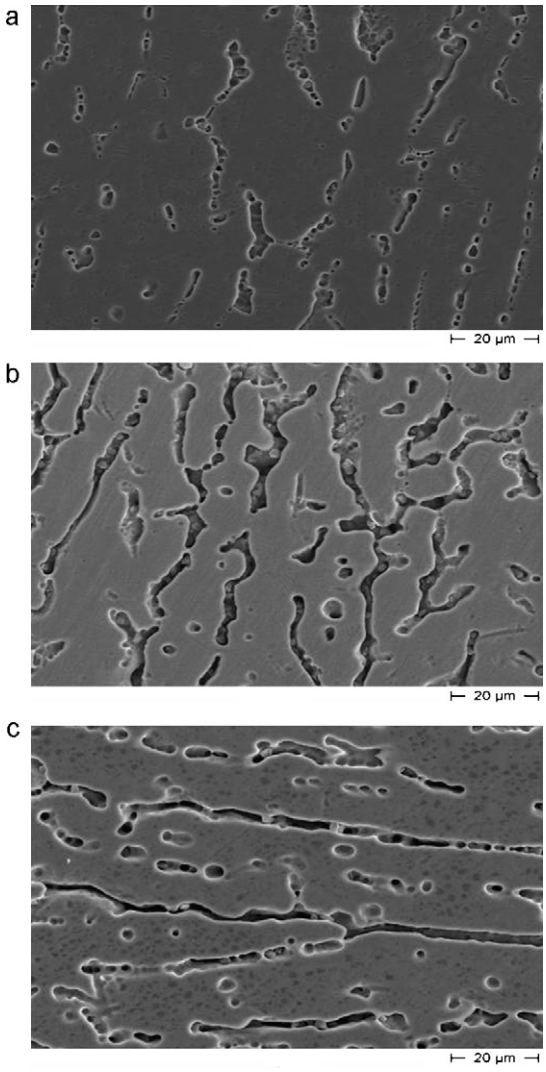

Fig. 1. Microstructure of the investigated as-cast $Ti_{51}Ni_{49-x}Si_x$ SMAs (a) 0% Si, (b) 1% Si, and (c) 2% Si.

gated shape memory alloys were studied by using scanning electron microscope (SEM). The different phases existing in the structure were analyzed using energy dispersive X-ray spectrometry (EDS) attached in the SEM operated at 20 kV. Phase transformation behavior of cast specimens was investigated by differential scanning calorimetry (DSC) at a cooling and heating rate of 10 °C min^{-1} using a Perkin Elmer diamond DSC calorimeter. Moreover, X-ray diffraction (XRD) was carried out to identify the existing different phases in the structure by using Cu Kα radiation with a step-scanning in 2θ range of 10–150°. The hardness measurements were carried out using Vickers hardness tester as indicator to the mechanical properties for these investigated alloys.

3. Results and discussion

3.1. Microstructure investigation

Fig. 1(a–c) displays SEM microstructures of the as-cast $Ti_{51}Ni_{49}$, $Ti_{51}Ni_{48}Si_1$ and $Ti_{51}Ni_{47}Si_2$ alloys, respectively. For the $Ti_{51}Ni_{49}$ alloy, the majority of the structure is composed of martensite phase (B19′) with austenite phase (B2) as minority and some precipitates of Ti_2Ni. While the other two investigated alloys that contained Si, the structures have also the same constituents as the first alloy and there is other some precipitates of intemetallic compound of $Ti_2(Ni + Si)$ in matrix. The dark phase in the microstructure is mainly located at the grain boundaries of the matrix, while the grey precipitated particles are essentially distributed inside the matrix.

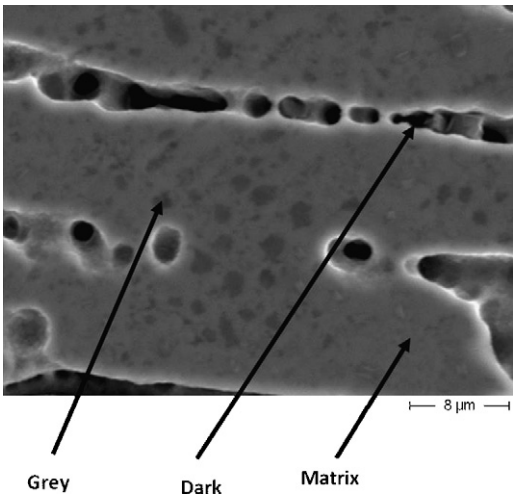

Fig. 2. Phases identification in the microstructure of as-cast $Ti_{51}Ni_{47}Si_2$ alloy.

Fig. 2 shows the microstructure of $Ti_{51}Ni_{47}Si_2$ alloy with higher magnification in order to display the different phases existing in its structure. It is obvious that there are two types of precipitated particles in the matrix. The first particle has a dark color that can be defined as Ti_2Ni and the second one has a grey color which is an intermetallic compound of $Ti_2(Ni + Si)$. The chemical composition of the matrix, dark and grey phases are given in Table 1. The data given in Table 1 are the averages that taken of at least five tests for each area with errors.

The volume fraction of both dark phase located at matrix grain boundaries and grey particles existing inside the matrix are increased with increasing Si content. It is noticed that the grey particles do not appear in the first cast alloy with no Si-addition (Ti_{51}–Ni_{49}–Si_0), while those grey particles start to appear by adding Si to the Ti–Ni alloy. The volume fraction of these grey particles is increased with increasing the Si-content, where their volume fractions were 2.33% for the second alloy (Ti_{51}–Ni_{48}–Si_1) and increased to 5.73 for the third cast alloy (Ti_{51}–Ni_{47}–Si_2).

According to TiNiSi ternary phase diagram [17] at temperatures between 750 and 1000 °C and chemical analysis obtained by EDS shown in Table 1 as well as the XRD pattern of the as-cast $Ti_{51}Ni_{48-x}Si_x$ alloys shown in Fig. 3, it could be concluded that the matrix shown in Fig. 1 is B19′ martensite in addition to existing of a small amount of retained austenite. Moreover, the amount of Si-content in matrix as a solid solution increases with the increasing amount of Si in the $Ti_{51}Ni_{48-x}Si_x$ alloys. The Si-content in matrix of the $Ti_{51}Ni_{48}Si_1$ alloy is estimated as 0.27% and increased to 0.64% for $Ti_{51}Ni_{47}Si_2$ alloy, Table 1. It was also reported by Bertheville and Nishida [18,19] that $Ti_2(Ni + Si)$ precipitates may precipitate on few oxides Ti_2NiO_x, which has the same structure as TiNi and, therefore, they are difficult to be distinguished.

3.2. Phase transformation behavior

The transformation temperatures of the three investigated SMAs were determined by DSC. Fig. 4 shows a typical DSC plot. It is observed that the transformation peak become sharper with an addition of 2% Si to the TiNi alloy compared with the others without and with 1% Si. The reason for this change in transformation peaks is considered to be due to precipitation of $Ti_2(Ni + Si)$. In addition, the samples exhibit two characteristic transformation peaks, which are absorption peak associated with reverse martensitic transformation (B19′ → B2) up heating and exothermic peak associated with martensitic transformation (B2 → B19′) [20]. The critical transformation are listed in Table 2 and the correlation between Si-contents

Table 1
Composition of the different phases existing in as cast $Ti_{51}Ni_{49-x}Si_x$ SMAs.

Element		Ti (at.%)			Ni (at.%)			Si (at.%)		
Phases	Si, at.%	0	1	2	0	1	2	0	1	2
Grey phase		63.93	65.71	65.68	36.07	33.82	32.86	0.00	0.47	1.46
Dark phase		64.18	66.45	66.95	35.82	33.52	33.01	0.00	0.03	0.04
Matrix		51.91	51.87	52.10	48.09	47.86	47.26	0.00	0.27	0.64

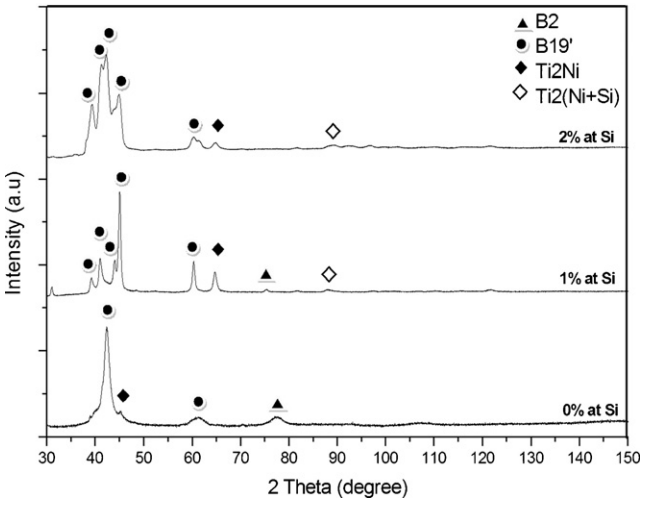

Fig. 3. XRD patterns of the samples with different Si contents showing the phase constituent.

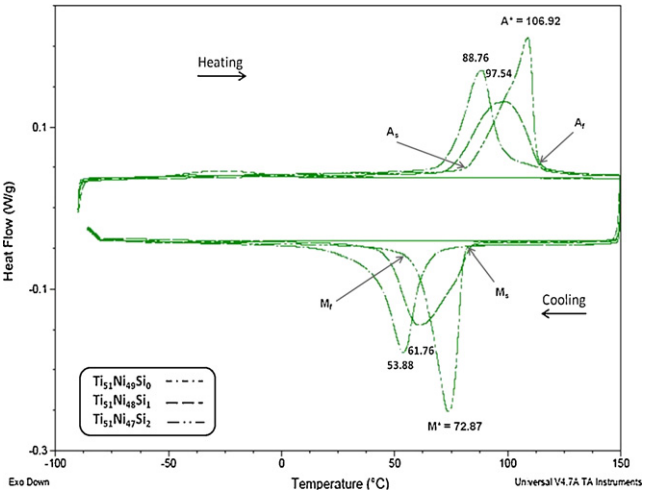

Fig. 4. Differential scanning calorimetry (DSC) curves of the investigated alloys. (a) Ti_{51}–Ni_{49}–Si_0, (b) Ti_{51}–Ni_{48}–Si_1, and (c) Ti_{51}–Ni_{47}–Si_2.

and the peak temperatures (M^* and A^*) for martensitic transformation are seen in Fig. 5. It is clear that the peak temperatures for both A^* and M^* increased with increasing the Si-content. This could be explained that silicon is considered an exothermic element; therefore increasing Si-contents in the TiNi alloy will increase the peak temperatures.

Table 2
Measured differential scanning calorimetry (DSC) transformation temperatures.

Alloy	A_s (°C)	A^*	A_f (°C)	M_s (°C)	M^*	M_f (°C)
$Ti_{51}Ni_{49}Si_0$	72.50	88.76	98.00	65.00	53.88	43.00
$Ti_{51}Ni_{48}Si_1$	75.01	97.54	114.50	82.50	61.76	47.50
$Ti_{51}Ni_{47}Si_2$	83.00	106.92	116.40	83.50	72.87	60.12

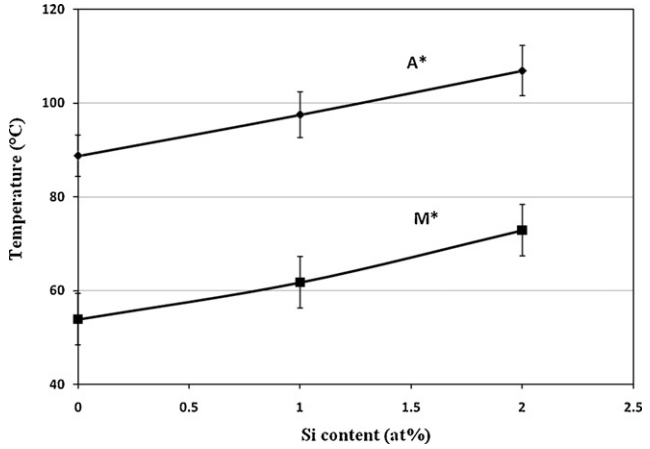

Fig. 5. Peak transformation temperatures of M^* and A^* vs. Si content for the as-cast TiNiSi SMAs.

Table 3
R ratio of Ti/(Ni + Si) for the as-cast $Ti_{51}Ni_{48-x}Si_x$ SMAs.

Ti/Ni in the matrix, *R*	Si (at.%)		
	0	1	2
R ratio	1.073	1.078	1.086

Moreover, the correlation between Ti, Ni and Si is formulated as *R*-ratio [where, *R* = Ti/(Ni + Si)] and plotted against transformation temperatures, as given in Table 3 and Fig. 6. It is clear that all transformation temperatures (A_s, A_f, M_s and M_f) are increased with increasing the *R*-ratio. These results were in agreement with the work done by Hseih et al. [21], i.e., they found the same relationship between *R*-ratio and transformation temperatures.

3.3. Hardness measurements

The hardness measurement gives a good indication about the mechanical properties of the as-cast $Ti_{51}Ni_{49-x}Si_x$ alloys and illustrating the effect of adding Si to TiNi alloy system. Fig. 7 shows the

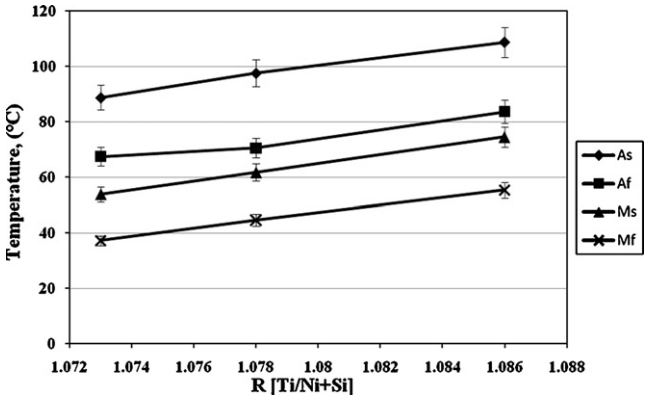

Fig. 6. Transformation of A_s, A_f, M_s and M_f vs. *R* ratio of as cast TiNiSi SMAs.

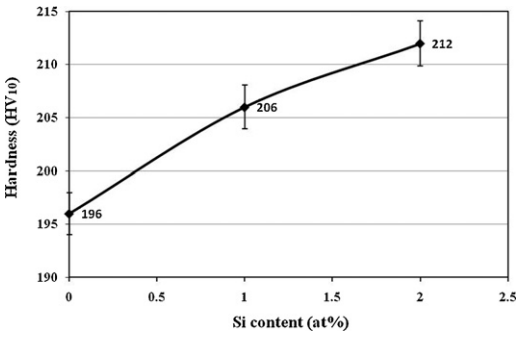

Fig. 7. Hardness measurements versus Si content, at.%.

hardness measurements of the as-cast $Ti_{51}Ni_{49-x}Si_x$ alloys against Si-content. The hardness value of $Ti_{51}Ni_{49}Si_0$ alloy is 196 HV_{10}, while the hardness for $Ti_{51}Ni_{48}Si_1$ and $Ti_{51}Ni_{47}Si_2$ alloys are 206 and 212 HV_{10}, respectively. This means that hardness is increased as the Si content increases in the TiNi alloys. This increment in hardness could be attributed to the precipitation of Ti_2(Ni, Si) particles in matrix.

As was shown in Fig. 1, the volume fraction of Ti_2(Ni, Si) particles is increased with the amount of Si content, which in turn affect the hardness measurements of the as-cast $Ti_{51}Ni_{49-x}Si_x$ alloys. In spite of increasing Si percentage in the solid solution and the volume fraction of Ti_2 (Ni, Si) precipitated particles in the matrix with Si content, the phase transformation peaks (A^* and M^*) are also increased in addition to the hardness of TiNiSi alloys, as was clear in Table 2, Figs. 5 and 7.

However Hseih [22] demonstrated that with increasing the amount of W in Ti-rich Ti_{51}–Ni_{49-x}–W_x, the transformation temperatures (A^* and M^*) decreased and the hardness values are increased. This phenomenon was also found in Ti-rich ($Ti_{52}Ni_{47}Al_1$) alloy. In the aforementioned alloy, this phenomenon was ascribed as W solid solution hardening mechanism. Therefore, the phenomenon of solid solution hardening mechanism can be also considered in the studied alloys [($Ti_{51}Ni_{48}Si_1$ and $Ti_{51}Ni_{47}Si_2$)]. It is pointed out that any strengthening mechanism that can impede transformation shear can also lower the M_s (M^*) transformation temperature because martensite transformation involves a shear process [23–25]. Moreover, martensitic transformation can be retarded by the fine hard dispersed particles, which may result in transformation temperatures being much more depressed. Si addition, like W, increases the percentage of precipitated fine particles in the matrix of TiNi system alloys, which in turn will retard martensitic transformation just like in case of W additions but vice versa it has a positive effect on enhancing the A^* and M^* transformation temperatures, unlike W additions.

4. Conclusion

This paper investigated the martensitic transformation and precipitated second phases as well as hardness of the cast $Ti_{51}Ni_{49-x}Si_x$ shape memory alloys. The conclusions are presented as the followings:

1. The microstructure of the as-cast $Ti_{51}Ni_{49-x}Si_x$ SMAs at room temperature consists of three phases in addition to the martensite phase B19′ matrix. The three phases are; a small amount of retained parent austenite phase B2, precipitated particles Ti_2Ni (dark phase) and intermetallic compound of Ti_2(Ni + Si) (grey phase).
2. DSC results indicate that the martensitic transformation reaction of the as-cast $Ti_{51}Ni_{49-x}Si_x$ SMAs is one stage B2 → B19′.
3. Forward martensitic reaction peak M^* and reverse martensitic transformation peak A^* are increased with increasing Si content. M^* and A^* were increased from 53.88 °C and 88.76 °C for the TiNi alloy without Si-addition to 61.76 °C and 97.54 °C with 1 at.% Si and 72.87 °C and 106.92 °C for 2 at.% Si alloy, respectively.
4. Hardness of the as-cast $Ti_{51}Ni_{49-x}Si_x$ SMAs is improved with increasing Si content. It is attributed to the increase of Si-content in the solid solution of the matrix and/or increasing the volume fraction of Ti_2Ni as well as Ti_2(Ni, Si) particles.

References

[1] S.D. Prokoshinkin, A.V. Korotitskiy, V. Brailovski, S. Turenne, I.Yu. Khmelevskaya, I.B. Trubitsyna, Acta Mater. 52 (2004) 4479.
[2] S.K. Wu, H.C. Lin, Mater. Chem. Phys. 64 (2000) 81.
[3] Y. Zheng, L. Cui, J. Schrooten, Appl. Phys. Lett. 84-1 (2004) 31.
[4] W.M. Huang, Mater. Sci. Eng. A 392 (2005) 121.
[5] T. Kurita, H. Matsumoto, H. Abe, J. Alloys Compd. 381 (2004) 158.
[6] D.C. Lagoudas, Shape Memory Alloys-Modeling and Engineering Applications, Springer Science + Busiress Media, LLC, 2008.
[7] D. Chrobak, D. Stroez, H. Morawiec, Scr. Mater. 48-5 (2003) 571.
[8] K. Otsuka, C.M. Wayman, Shape Memory Materials, Cambridge University Press, 1998.
[9] K.H. Eckelmeyer, Script. Metall. 10 (1976) 667.
[10] T. Honma, M. Matsumoto, Y. Shugo, M. Nishida, I. Yamazaki, in: H. Kimura, O. Izumi (Eds.), Proceedings 4th International Conference on Titanium'80, AIME, Warrendale, PA, 1980, p. 1455.
[11] C.M. Hwang, C.M. Wayman, Scripta Metallurgica 17 (3) (1983) 385.
[12] S.K. Wu, C.M. wayman, Metallography 20 (1987) 359.
[13] Y.C. Lo, S.K. Wu, C.M. Wayman, Script. Metall. 24 (1990) 1571.
[14] P.G. Lindqist, C.M. Wayman, in: T.W. Duering, K.N. Melton, D. Stockel, C.M. wayman (Eds.), Engineering Aspects of Shape Memory Alloys, Butterworth Heinmann, London, 1990, p. 58.
[15] H.C. Lin, S.K. Wu, J.C. Lin, Mater. Chem. Phys. 37 (1994) 184.
[16] Q. Hu, W. Jin, X.P. Liu, M.Z. Cao, S.X. Li, Mater. Lett. 54 (2002) 114.
[17] P. Villars, A. Prince, H. Okamoto, Handbook of Ternary Alloy Phase Diagrams, vol. 10, ASM International, Pittsburgh, USA, 1995, p. 13026.
[18] B. Bertheville, J.E. Bidaux, Sci. Mater. 52 (2005) 507.
[19] M. Nishida, C.M. Wayman, T. Honma, Metall. Trans. A 17 (1987) 785.
[20] S.F. Hseih, S.K. Wu, H.C. Lin, C.H. Yang, J. Alloys Compd. 387 (1–2) (2005) 121, 25.
[21] S.F. Hseih, S.K. Wu, H.C. Lin, J. Alloys Compd. 339 (2002) 162.
[22] S.F. Hseih, S.K. Wu, J. Mater. Sci. 34 (1999) 1665.
[23] M. Cohen, E.S. Machliin, V.G. Paranjpe, Thermodynamics in Physical Metallurgy, American Society for Metals, Metals Park, OH, 1950, p. 242.
[24] E. Hornbogen, Acta Metall. 33 (1985) 595.
[25] S. Eucken, E. Hornbogen, J. Mater. Sci. 19 (1984) 1343.